Molecular Orbital Studies of Zinc Oxide Chemical Vapor Deposition: Gas-Phase Radical Reactions

Barbara H. Munk and H. Bernhard Schlegel*

Department of Chemistry, Wayne State University, Detroit, Michigan, 48202

Received October 20, 2005. Revised Manuscript Received January 11, 2006

The gas-phase reactions involved in the radical mechanism for zinc oxide chemical vapor deposition have been examined by ab initio and density functional calculations. Geometries of reactants, transition structures, intermediate complexes, and products have been optimized with B3LYP/6-31G(d), and energetics have been computed with B3LYP/6-311+G(d,p), CCSD(T)/6-311+G(d,p), and MP2/6-311+G(3df,2p) levels of theory. The latter two were combined to give a G2(MP2)-like estimate of the enthalpy and free energy. Initiation reactions involve the thermal dissociation of diethyl zinc. The second bond dissociation of diethyl zinc is calculated to be significantly smaller than experimental estimates. The first step in the propagation reactions is ethyl radical abstracting a hydrogen from water to form hydroxyl radical. This has the highest barrier of the reaction sequence and would appear to be the rate-limiting step. The addition of hydroxyl radical to diethyl zinc proceeds without a barrier producing ethyl zinc hydroxide and regenerates ethyl radical. A similar set of propagation reactions converts ethyl zinc hydroxide to zinc dihydroxide. Additional propagation reactions involving oxyzinc radicals were also investigated. The gas-phase intermediates can react further to produce linear and cyclic oligomers. Comparison of the gas-phase reactions in the radical and closed shell mechanisms for zinc oxide chemical vapor deposition shows that the barrier heights for the rate-limiting steps are very similar.

Introduction

Zinc oxide thin films are wide band gap semiconductors that have received considerable attention because of desirable properties such as good conductivity and high transparency in the visible region.[1,2] These features make ZnO thin films very suitable as transparent electrodes for solar cells and as replacements for tin oxide films.[1] ZnO thin films can be deposited by atmospheric pressure chemical vapor deposition (CVD) of diethyl zinc and an oxygen source such as water at temperatures from 350 to 500 °C.[3−5] Zinc acetate,[6] zinc acetylacetonate,[7] and zinc amide[8] have also been used in ZnO CVD. Similar CVD schemes have been used to grow zinc sulfide and zinc selenide thin films.[9]

Interest in zinc oxide has increased with the recent development of "one-dimensional" zinc oxide nanostructures which have unique optical and electrical properties. Zinc oxide nanowires, nanobelts, nanotubes, and other nanostructures may have application in the development of sensors, actuators, and other optical devices.[10−13] Methods for preparing these zinc nanostructures include vapor−liquid−solid (VLS) processes, CVD, and the sol−gel process.

In a previous study related to zinc oxide chemical vapor deposition, we examined the closed shell gas-phase hydrolysis of diethyl zinc.[14] Calculations with density functional methods showed that $Zn(C_2H_5)_2$ hydrolysis by a single water has a barrier of 19 kcal/mol, but a second molecule of water lowers this barrier to 4 kcal/mol. Further hydrolysis of $Zn(C_2H_5)OH$ to $Zn(OH)_2$ is facile. Elimination of C_2H_6 or H_2O to form ZnO is very endothermic. $Zn(C_2H_5)OH$ and $Zn(OH)_2$ form very stable dimers and tetramers. Elimination of C_2H_6 and H_2O from the dimers and tetramers is also endothermic and leads to ring opening.

Closed shell gas-phase reactions are known to be important at lower temperatures. Studies of ZnSe CVD from $Zn(CH_3)_2$ and H_2Se indicate that free radical reactions dominate at the higher temperatures used in some CVD processes.[15−17] In particular, H atom and CH_3 radical act in a catalytic fashion in a radical chain mechanism that forms large ZnSe adducts. In the present paper, we use density functional theory and G2(MP2)-like calculations to examine various radical pathways that may be involved in the chemical vapor deposition of ZnO from diethyl zinc.

(1) Gordon, R. G. *MRS Bull.* **2000**, *25*, 52−57.
(2) Gleizes, A. N. *Chem. Vap. Deposition* **2000**, *6*, 155−173.
(3) Hu, J. H.; Gordon, R. G. *J. Appl. Phys.* **1992**, *72*, 5381−5392.
(4) Hu, J. H.; Gordon, R. G. *J. Electrochem. Soc.* **1992**, *139*, 2014−2022.
(5) Hu, J. H.; Gordon, R. G. *J. Appl. Phys.* **1992**, *71*, 880−890.
(6) Maruyama, T.; Shionoya, J. *J. Mater. Sci. Lett.* **1992**, *11*, 170−172.
(7) Minami, T.; Sonohara, H.; Takata, S.; Sato, H. *Jpn. J. Appl. Phys.* **1994**, *33*, L743−L746.
(8) Suh, S.; Miinea, L. A.; Hoffman, D. M.; Zhang, Z.; Chu, W. K. *J. Mater. Sci. Lett.* **2001**, *20*, 115−118.
(9) Jones, A. C.; O'Brien, P. *CVD of Compound Semiconductors.* VHC: Weinheim, Germany, 1997.
(10) Goldberger, J.; Sirbuly, D. J.; Law, M.; Yang, P. *J. Phys. Chem. B* **2005**, *109*, 9−14.
(11) Shen, G.; Bando, Y.; Lee, C. J. *J. Phys. Chem. B* **2005**, *109*, 10779−10785.
(12) Shen, G. Z.; Bando, Y.; Lee, C. J. *J. Phys. Chem. B* **2005**, *109*, 10578−10583.
(13) Song, J. H.; Wang, X. D.; Riedo, E.; Wang, Z. L. *J. Phys. Chem. B* **2005**, *109*, 9869−9872.
(14) Smith, S. M.; Schlegel, H. B. *Chem. Mater.* **2003**, *15*, 162−166.
(15) Cavallotti, C.; Moscatelli, D.; Carra, S. *J. Phys. Chem. A* **2004**, *108*, 1214−1223.
(16) Cavallotti, C.; Masi, M.; Lovergine, N.; Prete, P.; Mancini, A. M.; Carra, S. *J. Phys. IV* **1999**, *9*, 33−40.
(17) Moscatelli, D.; Cavallotti, C.; Masi, M.; Carra, S. *J. Cryst. Growth* **2003**, *248*, 31−36.

10.1021/cm052314x CCC: $33.50
Published on Web 03/08/2006

Table 1. Bond Dissociation Energies for Diethyl Zinc and Dimethyl Zinc (kcal/mol)

level of theory	$ZnR_2 \rightarrow Zn + 2R$	$ZnR_2 \rightarrow ZnR + R$	$ZnR \rightarrow Zn + R$
$Zn(CH_3)_2$ dissociation			
B3LYP/6-311G(d)[a]	86.8	78.7	8.1
B3LYP/6-311+G(d,p)[b]	76.6	64.8	11.8
B3LYP/6-311+G(3df,2p)[b]	77.0	64.9	12.1
MP2/6-311+G(d,p)[b]	89.4	72.1	17.2
MP2/6-311+G(3df,2p)[b]	93.3	75.0	18.3
MP3/6-311+G(d,p)[b]	78.0	65.8	12.1
CCSD(T)/6-311+G(d,p)[b]	79.8	67.0	12.8
CCSD(T)/6-311+G(3df,2p)	83.9	69.6	14.3
G2/MP2[b]	81.5	67.6	13.9
experimental[29]	88.8	68.0	20.8
experimental[31]	81.9-88.1	69.4	12.5-18.7
experimental[30]	88.2	63.7	24.5
$Zn(C_2H_5)_2$ dissociation			
B3LYP/6-311G(d)[a]	73.4	68.9	4.5
B3LYP/6-311+G(d,p)[a]	61.0	55.0	6.0
B3LYP/6-311+G(d,p)[b]	61.2	55.1	6.2
MP2/6-311+G(d,p)[a]	79.1	66.9	12.2
MP2/6-311+G(3df,2p)[a]	83.0	69.6	13.5
MP3/6-311+G(d,p)[a]	65.9	59.1	6.8
CCSD(T)/6-311+G(d,p)[a]	68.5	60.4	8.1
G2/MP2[a]	69.5	60.2	9.3
experimental[29]	73.9	56.1	18.2
experimental [30]	74.4	52.4	22.0

[a] Geometry optimized at B3LYP/6-311G(d). [b] Geometry optimized at B3LYP/6-311+G(d,p).

Method

Molecular orbital calculations were carried out using the development version of the GAUSSIAN series of programs.[18] Equilibrium geometries were optimized by the B3LYP density functional method[19−21] using the 6-311G(d) basis set[22−26] (for zinc, this corresponds to the 14s,9p,5d Wachters-Hay basis set[24−26] contracted to 9s,5p,3d and augmented with an f-type Gaussian shell with an exponent of 1.620). Selected structures were also optimized with larger basis sets and higher levels of theory. Since the open-shell systems showed very little spin contamination ($S^2 = 0.75-0.81$), the spin-unrestricted energies were used without spin projection. Vibrational frequencies were computed at the B3LYP/6-311G(d) level and were used without scaling since the B3LYP frequencies agree quite well with experimental values for a wide range of second and third period compounds.[27] Thermal corrections and entropies were calculated by standard statistical thermodynamic methods[28] using the unscaled B3LYP frequencies and the ideal gas/rigid rotor/harmonic oscillator approximations. To obtain more accurate energetics, single-point calculations were carried out at the B3LYP/ 6-311G(d) optimized geometry using the B3LYP/6-311+G(d,p), MP2/6-311+G(d,p), MP2/6-311+G(3df,2p), and CCSD(T)/6-311+G(d,p) levels of theory. Data from the later levels of theory were combined using a G2(MP2)-type approach

$$E(\text{total}) = E(\text{CCSD(T)/6-311+G(d,p)}) + E(\text{MP2/6-311+G(3df,2p)}) - E(\text{MP2/6-311+G(d,p)}) + \text{HLC} + \text{ZPE(B3LYP/6-311G(d))}$$

with the higher level correction given by $\text{HLC} = -0.00481n_\alpha - 0.000019n_\beta$, where n_α and n_β are the number of valence α and β electrons. The G2(MP2)-like energy differences in the present work are anticipated to have a mean absolute deviation of ca. 5 kcal/mol when compared to experiment.

Results and Discussion

Radical chain reactions involve initiation, propagation, and termination steps. Comparison with radical mechanisms for ZnS and ZnSe deposition suggests that the chain carriers for ZnO CVD from diethyl zinc could include ethyl radical, hydroxyl radical, and hydrogen atom. In the gas phase, thermal initiation will proceed by cleavage of the weakest bond. In the present case, these are the Zn−C bonds in $Zn(C_2H_5)_2$. The O−H and C−H bond energies are considerably higher, and this probably precludes hydrogen atom as a chain carrier. Because of the weakness of the Zn−C bond in ZnC_2H_5 (see data in Table 1), it is unlikely that ZnC_2H_5 is a chain carrier. In the propagation steps, ethyl radical can react with water to produce hydroxyl radical, which can in turn attack diethyl zinc, regenerating ethyl radical. A simple gas-phase radical mechanism for the formation of $Zn(OH)_2$ can be can be constructed from the following reactions:

(18) Frisch, M. J.; Trucks, G. W.; Schlegel, H. B.; Scuseria, G. E.; Robb, M. A.; Cheeseman, J. R.; Montgomery, J. A.; Vreven, T.; Kudin, K. N.; Burant, J. C.; Millam, J. M.; Iyengar, S.; Tomasi, J.; Barone, V.; Mennucci, B.; Cossi, M.; Scalmani, G.; Rega, N.; Petersson, G. A.; Nakatsuji, H.; Hada, M.; Ehara, M.; Toyota, K.; Fukuda, R.; Hasegawa, J.; Ishida, M.; Nakajima, T.; Honda, Y.; Kitao, O.; Nakai, H.; Klene, M.; Li, X.; Knox, J. E.; Hratchian, H. P.; Cross, J. B.; Adamo, C.; Jaramillo, J.; Gomperts, R.; Stratmann, R. E.; Yazyev, O.; Austin, A. J.; Cammi, R.; Pomelli, C.; Ochterski, J.; Ayala, P. Y.; Morokuma, K.; Voth, G. A.; Salvador, P.; Dannenberg, J. J.; Zakrzewski, V. G.; Dapprich, S.; Daniels, A. D.; Strain, M. C.; Farkas, Ö.; Malick, D. K.; Rabuck, A. D.; Raghavachari, K.; Foresman, J. B.; Ortiz, J. V.; Cui, Q.; Baboul, A. G.; Clifford, S.; Cioslowski, J.; Stefanov, B. B.; Liu, G.; Liashenko, A.; Piskorz, P.; Komaromi, I.; Martin, R. L.; Fox, D. J.; Keith, T.; Al-Laham, M. A.; Peng, C. Y.; Nanayakkara, A.; Challacombe, M.; Gill, P. M. W.; Johnson, B.; Chen, W.; Wong, M. W.; Andres, J. L.; Gonzalez, C.; Replogle, E. S.; Pople, J. A. *Gaussian 03*, Gaussian 03.A1; Gaussian, Inc.: Pittsburgh, PA, 2003.
(19) Becke, A. D. *Phys. Rev. A* **1988**, *38*, 3098−3100.
(20) Becke, A. D. *J. Chem. Phys.* **1993**, *98*, 5648−5652.
(21) Lee, C.; Yang, W.; Parr, R. D. *Phys. Rev. B* **1988**, *37*, 785−789.
(22) Krishnan, R.; Binkley, J. S.; Seeger, R.; Pople, J. A. *J. Chem. Phys.* **1980**, *72*, 650.
(23) McLean, A. D.; Chandler, G. S. *J. Chem. Phys.* **1980**, *72*, 5639.
(24) Wachters, A. J. H. *J. Chem. Phys.* **1970**, *52*, 1033.
(25) Hay, J. P. *J. Chem. Phys.* **1977**, *66*, 4377.
(26) Raghavachari, K.; Trucks, G. W. *J. Chem. Phys.* **1989**, *91*, 1062−1065.
(27) Scott, A. P.; Radom, L. *J. Phys. Chem.* **1996**, *100*, 16502−16513.
(28) McQuarrie, D. A. *Statistical Thermodynamics*; University Science Books: Mill Valley, CA, 1973.

$$Zn(C_2H_5)_2 \rightarrow ZnC_2H_5 + \bullet C_2H_5 \quad \text{(initiation)} \quad (1)$$

$$ZnC_2H_5 \rightarrow Zn + \bullet C_2H_5 \quad \text{(initiation)} \quad (2)$$

$$H_2O + \bullet C_2H_5 \rightarrow C_2H_6 + \bullet OH \quad \text{(propagation)} \quad (3)$$

$$Zn(C_2H_5)_2 + \bullet OH \rightarrow Zn(OH)C_2H_5 + \bullet C_2H_5 \quad \text{(propagation)} \quad (4)$$

$$Zn(OH)C_2H_5 + \bullet OH \rightarrow Zn(OH)_2 + \bullet C_2H_5 \quad \text{(propagation)} \quad (5)$$

$$\bullet OH + \bullet C_2H_5 \rightarrow C_2H_5OH \quad \text{(termination)} \quad (6)$$

$$2\bullet C_2H_5 \rightarrow C_4H_{10} \quad \text{(termination)} \quad (7)$$

In addition to the propagation steps 3−5, the gas-phase radical mechanism could include attack of the ethyl radical at a water molecule bound to the diethyl zinc and ethyl radical abstracting a hydrogen from zinc dihydroxide or ethyl zinc hydroxide.

The relative energies of the gas-phase reactants, intermediates, products, and transition states are listed in Table 2. Figures 1−3 show the structures and key geometric parameters of some of the important intermediates and transition states in the propagation reactions. Figures 4 and 5 provide energy profiles for these reaction steps.

Initiation Reactions. Bond dissociation energies for dimethyl and diethyl zinc are collected in Table 1 and serve to calibrate the theoretical methods. The experimental values for overall dissociation energy are 81.9−88.8 kcal/mol for dimethyl zinc[29−31] and 73.9−74.4 kcal/mol for diethyl zinc.[29,30] At first sight, the values calculated at the B3LYP/6-311G(d) level of theory, 86.8 kcal/mol for dimethyl zinc and 73.4 kcal/mol for diethyl zinc, appear to be in excellent agreement with experiment. However, addition of diffuse functions lowers the overall bond dissociation energies by ca. 10 kcal/mol. Increasing the number of polarization functions [6-311+G(d,p) → 6-311+G(3df,2p)] changes the B3LYP dissociation energies of $Zn(CH_3)_2$ by less than 0.5 kcal/mol. Optimization of the geometry at B3LYP/6-311G(d) versus B3LYP/6-311+G(d,p) changes the B3LYP/6-311+G(d,p) dissociation energies of $Zn(C_2H_5)_2$ by less than 0.2 kcal/mol. In terms of geometry and basis set effects, it appears that computing B3LYP/6-311+G(d,p) energies at B3LYP/6-311G(d) optimized geometries is a satisfactory protocol for these density functional calculations. Since the B3LYP

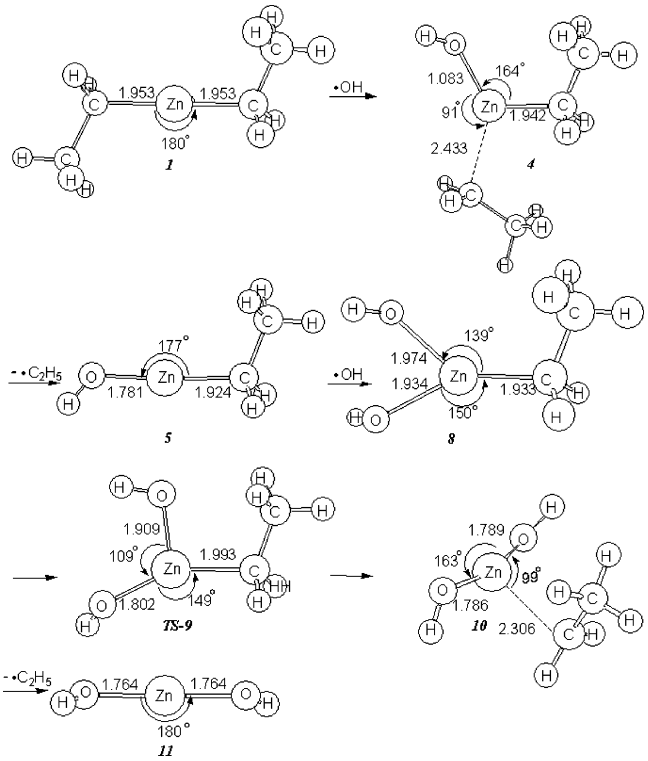

Figure 1. Structures and geometries of intermediates in the propagation reactions.

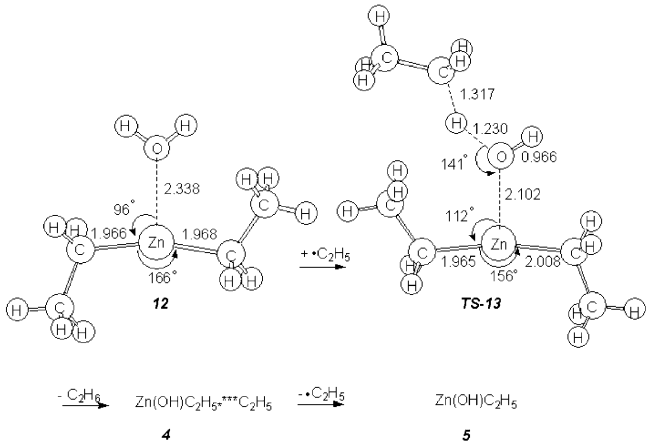

Figure 2. Structures and geometries of intermediates in the additional propagation reactions.

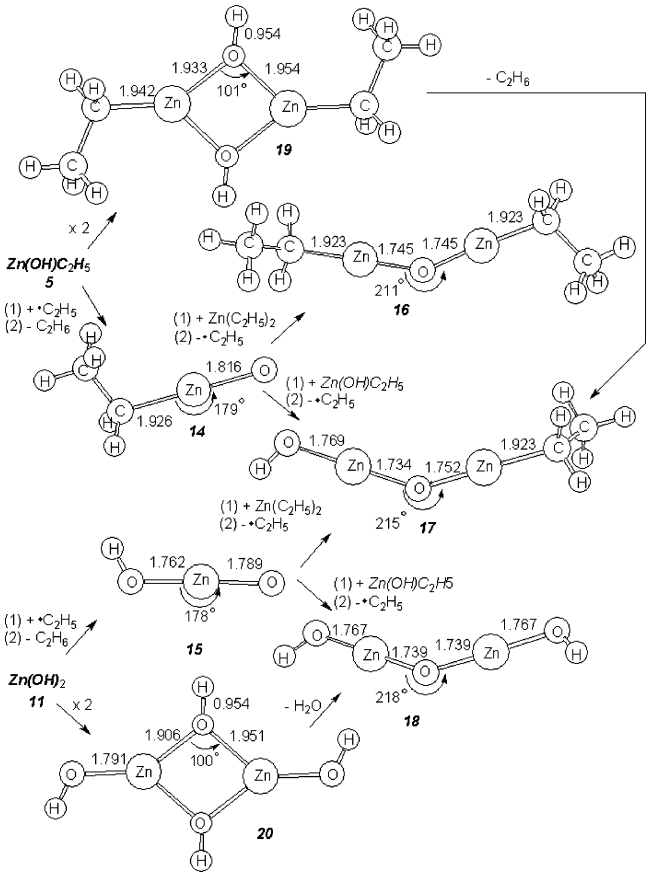

Figure 3. Structures and geometries of intermediates in the additional propagation reactions.

Table 2. Relative Enthalpies and Free Energies for Gas-Phase Species in the Radical Mechanism for ZnO Chemical Vapor Deposition from Diethyl Zinc and Water (kcal/mol)[a]

		ΔH			ΔG	
no.		G2/MP2 298 K 1 atm	B3LYP/ 6-311+G(d,p) 298 K 1 atm	B3LYP/ 6-311G(d) 298 K 1 atm	G2 (MP2) energies 700 K 10 Torr (1 atm)	B3LYP/6-311+G(d,p) energies 700 K 10 Torr (1 atm)
	propagation reactions					
1	$2Zn(C_2H_5)_2 + \bullet C_2H_5 + 4H_2O$	0.0	0.0	0.0	0.0	0.0
2	$2Zn(C_2H_5)_2 + 3H_2O + HO-H-C_2H_5$ (TS)	18.5	13.2	8.7	44.5 (38.6)	40.6 (34.8)
3	$2Zn(C_2H_5)_2 + C_2H_6 + 3H_2O + \bullet OH$	16.8	16.4	10.1	22.1	20.8
4	$Zn(OH)C_2H_5\cdots C_2H_5 + C_2H_6 + 3H_2O + Zn(C_2H_5)_2$	−22.3	−19.7	−20.3	7.3 (1.3)	7.7 (1.6)
5	$Zn(OH)C_2H_5 + \bullet C_2H_5 + C_2H_6 + 3H_2O + Zn(C_2H_5)_2$	−20.2	−20.5	−13.8	−22.7	−23.5
6	$Zn(OH)C_2H_5 + C_2H_6 + HO-H-C_2H_5$ (TS) $+ 2H_2O + Zn(C_2H_5)_2$	−1.7	−7.3	−5.1	21.8 (15.9)	17.1 (11.2)
7	$Zn(OH)C_2H_5 + 2C_2H_6 + 2H_2O + \bullet OH + Zn(C_2H_5)_2$	−3.4	−4.1	−3.7	−0.6	−2.8
8	$Zn(OH)_2C_2H_5 + 2C_2H_6 + 2H_2O + Zn(C_2H_5)_2$	−9.9	−19.6	−28.7	20.2 (14.2)	7.2 (1.2)
9	$Zn(OH)_2C_2H_5$ (TS) $+ 2C_2H_6 + 2H_2O + Zn(C_2H_5)_2$	−17.7	−21.9	−22.6	14.0 (8.0)	7.6 (1.6)
10	$Zn(OH)_2\cdots C_2H_5 + 2C_2H_6 + 2H_2O + Zn(C_2H_5)_2$	−36.3	−33.4	−35.4	−8.2 (−14.2)	−8.0 (−14.0)
11	$Zn(OH)_2 + \bullet C_2H_5 + 2C_2H_6 + 2H_2O + Zn(C_2H_5)_2$	−34.2	−33.7	−22.7	−38.1	−38.5
	$2Zn(OH)C_2H_5 + \bullet C_2H_5 + 2C_2H_6 + 2H_2O$	−40.4	−41.1	−27.6	−45.4	−47.0
	$Zn(OH)_2 + Zn(OH)C_2H_5 + \bullet C_2H_5 + 3C_2H_6 + H_2O$	−54.4	−54.3	−36.5	−60.8	−62.0
	$2Zn(OH)_2 + \bullet C_2H_5 + 4C_2H_6$	−68.4	−68.3	−45.4	−76.2	−77.0
	additional propagation reactions					
12	$Zn(C_2H_5)_2\cdot H_2O + C_2H_5 + 3H_2O + Zn(C_2H_5)_2$		−2.6	−7.0		19.6 (13.6)
13	$Zn(C_2H_5)_2\cdot HO-H-C_2H_5$ (TS) $+ 3H_2O + Zn(C_2H_5)_2$		6.1	−1.0		61.5 (49.5)
14	$Zn(C_2H_5)O\bullet + 2C_2H_6 + 3H_2O + Zn(C_2H_5)_2$		−5.2	−5.2		−2.9
14	$Zn(C_2H_5)O\bullet + 3C_2H_6 + 2H_2O + Zn(OH)C_2H_5$		−25.7	−19.0		−26.4
15	$HOZnO\bullet + \bullet C_2H_5 + 3C_2H_6 + 2H_2O + Zn(C_2H_5)_2$		−19.0	−14.0		−17.7
15	$HOZnO\bullet + \bullet C_2H_5 + 4C_2H_6 + H_2O + Zn(OH)C_2H_5$		−39.5	−27.8		−41.3
	linear and cyclic oligomers					
16	$(C_2H_5)ZnOZnC_2H_5 + \bullet C_2H_5 + 2C_2H_6 + 3H_2O$		−43.6	−26.0		−49.5
17	$HOZnOZnC_2H_5 + \bullet C_2H_5 + 3C_2H_6 + 2H_2O$		−57.2	−36.0		−63.5
18	$HOZnOZnOH + \bullet C_2H_5 + 4C_2H_6 + H_2O$		−70.2	−45.4		−76.4
19	cyclic $(Zn(OH)C_2H_5)_2 + \bullet C_2H_5 + 2C_2H_6 + 2H_2O$	−79.9	−73.2	−75.5	−50.1 (−56.1)	−46.0 (−52.0)
20	cyclic $(Zn(OH)_2)_2 + \bullet C_2H_5 + 4C_2H_6$	−111.1	−104. 0	−94.6	−84.1 (−90.1)	−80.3 (−86.4)
	closed shell reactions					
21	$Zn(C_2H_5)_2-H_2O$ (TS) $+ \bullet C_2H_5 + 3H_2O + Zn(C_2H_5)_2$	16.8	19.1	19.1	41.7 (35.7)	46.5 (40.4)
22	$Zn(OH)C_2H_5-H_2O$ (TS) $+ \bullet C_2H_5 + 2H_2O + Zn(C_2H_5)_2 + C_2H_6$	3.2	6.4	7.7	28.8 (22.7)	33.9 (27.9)

[a] All geometries were optimized at the B3LYP/6-311G(d) level of theory.

calculations appear to be ca. 10 kcal/mol lower than the experimental values, the bond dissociation energies were also calculated by the G2(MP2)-like approach. For the 6-311+G(d,p) basis, the MP3 and CCSD(T) values are similar but are ca. 10 kcal/mol lower than MP2, indicating that the MP2 values are too high for a given basis set. For dimethyl zinc dissociation, increasing the basis set from 6-311+G(d,p) to 6-311+G(3df,2p) changes the CCSD(T) values by essentially the same amount as the MP2 values, indicating that the basis set additivity approximation in the G2(MP2) approach is satisfied to ±0.5 kcal/mol or better. The CCSD(T)/6-311+G(d,p) level of theory is comparable to the QCISD(T)/cc-pVDZ calculations of Ortiz and co-workers[32] and yields similar bond dissociation energies (79.8 kcal/mol for CCSD(T) versus 82.7 kcal/mol for QCISD(T)). Taken together, these results indicate that the G2(MP2) level of theory is well-balanced in terms of treating basis set effects and electron correlation and should give reasonable estimates of relative energies. The propagation steps (reactions 3−5)

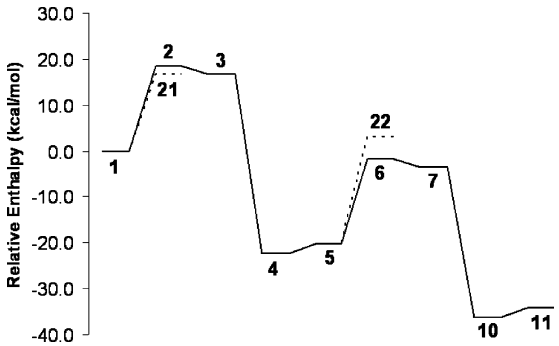

Figure 4. Potential energy profile showing relative enthalpies at 298 K and 1 atm for the radical propagation reactions calculated with the G2(MP2)-like level of theory (structures are provided in Figure 1 and Table 2). Dashed lines show the enthalpy barriers for the closed shell hydrolysis reactions.

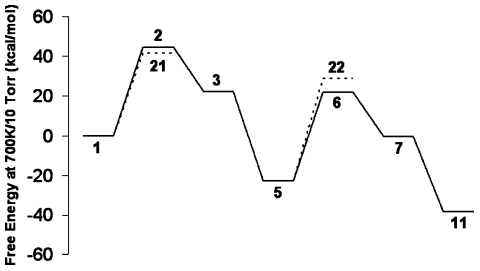

Figure 5. Potential energy profile showing relative free energies at 700 K and 10 Torr for the radical propagation reactions calculated with the G2(MP2)-like level of theory (structures are provided in Figure 1 and Table 2). Dashed lines show the free energy barriers for the closed shell hydrolysis reaction.

(29) Afeefy, H. Y. L.; Liebman, J. F.; Stein, S. E. Neutral Thermochemical Data. In *NIST Chemistry WebBook*; NIST Standard Reference Database Number 69; Mallard, W. G., Lindstrom, P. J., Eds.; National Institute of Science and Technology: in press.
(30) Jackson, R. L. *Chem. Phys. Lett.* **1989**, *163*, 315−322.
(31) Georgiadis, R.; Armentrout, P. B. *J. Chem. Am. Soc.* **1986**, *108*, 2119−2126.
(32) Zakrzewski, V. G.; Ortiz, J. V. *J. Chem. Phys.* **1994**, *100*, 6508−6513.

should be less sensitive to the level of theory than the bond dissociations in the initiation steps (reactions 1 and 2), since for every bond broken another bond is formed, thereby partially canceling the remaining errors in the calculated bond energies.

The overall bond dissociation energies at the B3LYP/6-311+G(d,p) and G2(MP2) levels of theory are 76.6 and 81.5 kcal/mol, respectively, for dimethyl zinc and 61.2 and 69.5 kcal/mol for diethyl zinc. The B3LYP values are 5−13 kcal/mol lower than experiment, while the G2(MP2) values are only 1−7 kcal/mol lower. However, there is agreement between experiment and all the calculations in Table 1 that the dissociation energy of diethyl zinc is 10−15 kcal/mol lower than dimethyl zinc. Density functional calculations of dimethyl zinc bonded to a cluster model of a Zn−S surface indicate that the Zn−C dissociation energy could be significantly lower on a surface than in the gas phase.[33]

For diethyl zinc, the published experimental values for the first and second bond dissociation energies are 52.4−56.1 and 18.2−22.0 kcal/mol, respectively.[29,30] The calculated values are 55.1 and 6.2 kcal/mol by B3LYP/6-311+G(d,p) and 60.2 and 9.3 kcal/mol by G2(MP2). A similar situation is found for dimethyl zinc. Experimental values are 68.0 and 20.8 kcal/mol,[29] while the calculated values are 64.8 and 11.8 kcal/mol by B3LYP/6-311+G(d,p), 67.6 and 13.9 kcal/mol by G2(MP2), and 69.6 and 13.1 kcal/mol by QCISD(T)/cc-pVDZ.[32] The calculations strongly suggests that the second bond dissociation energies in both dimethyl and diethyl zinc are smaller than the reported experimental values. In situations where the second bond dissociation energy is much smaller than the first, it is difficult experimentally to determine the individual dissociation energies, even if the sum of the dissociation energies can be obtained reliably.

Because of the small second bond dissociation energy, the initiation step via thermal dissociation of diethyl zinc yields a zinc atom and two ethyl radicals. The ethyl radicals can participate directly in the chain reaction. The zinc atom can react further with water to produce HZnOH,[34−36] ZnOH + H, and $Zn(OH)_2$ + 2H. While the former reaction is exothermic by 0.8 kcal/mol at B3LYP/6-311+G(d,p) and 3.9 kcal/mol at G2(MP2), the latter two reactions are endothermic by 77.1 and 101.9 kcal/mol at B3LYP/6-311+G(d,p) and 69.9 and 86.0 kcal/mol at G2(MP2). The latter reactions are therefore unlikely to contribute chain carriers to the propagation reactions.

Propagation Reactions. The first propagation step, (3), is the reaction between ethyl radical and water. Because O−H bonds are stronger than C−H bonds, this reaction is endothermic by 18.7 kcal/mol.[29] By contrast, for ZnS and ZnSe deposition, the corresponding steps are exothermic since the S−H and Se−H bonds are weaker than C−H bonds. The B3LYP/6-311+G(d,p) and G2(MP2) calculations underestimate the reaction enthalpy by 2 kcal/mol. The reverse reaction, $C_2H_6 + \bullet OH \rightarrow H_2O + \bullet C_2H_5$, has a low activation energy (2.1−2.2 kcal/mol at 298 K)[37,38] and a small classical barrier (4.0 kcal/mol).[39] Calculations with B3LYP/6-311+G(d,p) and G2(MP2) underestimated the classical barrier for the reverse reaction by 5.4 and 0.2 kcal/mol, respectively. Reoptimization of the transition state with B3LYP/6-311+G(d,p) increases the barrier height by less than 0.5 kcal/mol.

Alternatively, if hydrogen is used as a carrier gas, ethyl radical could react with H_2 to produce ethane and hydrogen atom. The B3LYP/6-311+G(d,p) and G2(MP2) calculations indicate that this reaction is endothermic by 6.2 and 1.3 kcal/mol, respectively. This is consistent with the experimental value of 3.7 kcal/mol.[29] Both levels of theory underestimate the vibrationally adiabatic barrier height of the reverse reaction by 6.9 and 5.1 kcal/mol, respectively, when compared to higher level calculations (CCSD(T,full)/cc-pVTZ//MP2(full)/cc-pVTZ).[40] In a second step, hydrogen atom can react with water to form H_2 and •OH. This yields the same overall reaction as discussed in the previous paragraph, $\bullet C_2H_5 + H_2 + H_2O \rightarrow C_2H_6 + H_2 + \bullet OH$. The reverse of the second step has a classical barrier of 6.3 kcal/mol at the QCISD(T) level of theory with an additivity approximation for the basis set effect ($\Delta_{basis} = E$[MP2/6-311+G(2df,2dp)] − E[MP2/6-311G(d,p)]).[41] B3LYP/6-311+G(d,p) and G2(MP2) estimate the barrier height at 1.0 and 2.8 kcal/mol, respectively. At both levels of theory, the enthalpic barrier heights for the two-step reaction are 3.2 (B3LYP/6-311+G(d,p)) and 1.1 (G2(MP2)) kcal/mol higher than those calculated for the direct reaction between ethyl radical and water. This suggests that both pathways may contribute to the first propagation step, with the direct reaction somewhat more favorable than the indirect reaction. The back-reaction, $H_2 + \bullet OH \rightarrow H + H_2O$, may deplete the amount of hydroxyl radical that can proceed to react with diethyl zinc.

The next step in the chain reaction, (4), is the attack of hydroxyl radical on diethyl zinc, **1**. Reaction path following at the B3LYP/6-311G(d) level of theory shows that the reaction proceeds without a barrier—as the hydroxyl radical approaches the diethyl zinc, the energy decreases monotonically until the reaction reaches complex **4**. The reaction of $Zn(C_2H_5)_2 + \bullet OH \rightarrow Zn(OH)C_2H_5\cdots C_2H_5$ is exothermic by 38.9 kcal/mol at the G2(MP2)-like level of theory. This complex consists of ethyl zinc hydroxide loosely coordinated with an ethyl radical at a distance of 2.43 Å and bound by 2.1 kcal/mol at the G2(MP2) level of theory, respectively. Dissociation of **4** produces ethyl zinc hydroxide, **5**, and ethyl radical. The latter can react with water to regenerate a hydroxyl radical, as in the first propagation step.

The final propagation step, (5), is the addition of hydroxyl radical to ethyl zinc hydroxide. Optimizations at the MP2/6-311G(d), B3LYP/6-311G(d), and B3LYP/6-311+G(d,p)

(33) Cavallotti, C.; Moscatelli, D.; Masi, M.; Carra, S. *J. Cryst. Growth* **2004**, *266*, 363−370.
(34) Greene, T. M.; Brown, W.; Andrews, L.; Downs, A. J.; Chertihin, G. V.; Runeberg, N.; Pyykko, P. *J. Phys. Chem.* **1995**, *99*, 7925−7934.
(35) Kauffman, J. W.; Hauge, R. H.; Margrave, J. L. *J. Phys. Chem.* **1985**, *89*, 3541−3547.
(36) Macrae, V. A.; Greene, T. M.; Downs, A. J. *Phys. Chem. Chem. Phys.* **2004**, *6*, 4586−4594.
(37) Atkinson, R. *J. Phys. Chem. Ref. Data, Monogr.* **1989**, *1*, 18.
(38) Abbatt, J. P. D.; Demerjian, K. L.; Anderson, J. G. *J. Phys. Chem.* **1990**, *94*, 4566−4575.
(39) Melissas, V. S.; Truhlar, D. G. *J. Phys. Chem.* **1994**, *98*, 875−886.
(40) Kerkeni, B.; Clary, D. C. *J. Chem. Phys.* **2005**, *123*.
(41) Bettens, R. P. A.; Collins, M. A.; Jordan, M. J. T.; Zhang, D. H. *J. Chem. Phys.* **2000**, *112*, 10162−10172.

levels of theory predict the barrierless addition of •OH to $Zn(OH)C_2H_5$ to form a tricoordinated zinc radical complex, $Zn(OH)_2C_2H_5$, **8**. The calculated •OH binding energy is −15.8 kcal/mol at the B3LYP/6-311+G(d,p) level of theory. However, the barrier for the dissociation of $Zn(OH)_2C_2H_5$ via transition state **9** to the complex of zinc hydroxide with ethyl radical, **10**, is only 1.1 kcal/mol when optimized at B3LYP/6-311+G(d,p). This suggests that the tricoordinate zinc complex, **8**, may not exist at the G2(MP2) level of theory. Dissociation of complex **10** to form zinc dihydroxide, **11**, and ethyl radical is endothermic by 2.1 kcal/mol at the G2(MP2) level of theory.

Figure 4 summarizes the enthalpies of the gas-phase radical propagation reactions related to ZnO CVD. The enthalpy of the overall reaction, $Zn(C_2H_5)_2 + 2H_2O \rightarrow Zn(OH)_2 + 2C_2H_6$, is −33.7 and −34.2 kcal/mol at the B3LYP/6-311+G(d,p) and G2(MP2)-like levels of theory, respectively. When catalyzed by ethyl radical, the only endothermic step is generation of hydroxyl radical via $H_2O + •C_2H_5 \rightarrow C_2H_6 + •OH$. The remaining reactions involve the addition of hydroxyl radical to diethyl zinc and ethyl zinc hydroxide, and these proceed with little or no enthalpy barrier.

Termination Reactions. The gas-phase termination reactions 6 and 7 are radical recombination reactions, which are quite exothermic (80−90 kcal/mol) and can be expected to proceed with no enthalpic barrier. Other termination reactions would include reactions with the walls and with the growing film on the substrate.

Additional Propagation Reactions. Since the $H_2O + •C_2H_5 \rightarrow C_2H_6 + •OH$ propagation step (reaction 3) is endothermic and may be rate-determining, it is of interest to explore alternative pathways. One possibility is reaction 8, in which hydrogen abstraction occurs not from free water but from a water bound to the zinc oxide surface or bound to a molecule of diethyl zinc (structure **12** in Figure 2).

$$Zn(C_2H_5)_2•H_2O + •C_2H_5 \rightarrow Zn(OH)(C_2H_5)_2 + C_2H_6 \rightarrow Zn(OH)C_2H_5 + •C_2H_5 + C_2H_6 \quad (8)$$

The B3LYP/6-311+G(d,p) calculations show that the barrier from the complex is 4.5 kcal/mol lower than the abstraction barrier for free water. After the transition state, the bound hydroxyl radical proceeds to displace an ethyl group without further barrier. A similar process could occur on the growing zinc oxide surface.

Other alternative propagation reactions include ethyl radical abstracting a hydrogen from $Zn(OH)C_2H_5$ and $Zn(OH)_2$ to produce $•OZnC_2H_5$, **14**, and •OZnOH, **15**.

$$Zn(OH)C_2H_5 + •C_2H_5 \rightarrow (C_2H_5)ZnO• + C_2H_6 \quad (9)$$

$$Zn(OH)_2 + •C_2H_5 \rightarrow HOZnO• + C_2H_6 \quad (10)$$

At B3LYP/6-311+G(d,p), the enthalpy for these abstraction reactions are 15.3 and 14.7 kcal/mol, respectively, compared to 16.4 kcal/mol for abstraction from water (reaction 3). Analogous to hydroxyl radical, the resulting oxyzinc radicals can add to diethyl zinc and ethyl zinc hydroxide and regenerate ethyl radical.

$$(C_2H_5)ZnO• + Zn(C_2H_5)_2 \rightarrow (C_2H_5)ZnOZnC_2H_5 + •C_2H_5 \quad (11)$$

$$(C_2H_5)ZnO• + Zn(OH)C_2H_5 \rightarrow (C_2H_5)ZnOZnOH + •C_2H_5 \quad (12)$$

$$HOZnO• + Zn(C_2H_5)_2 \rightarrow (C_2H_5)ZnOZnOH + •C_2H_5 \quad (13)$$

$$HOZnO• + Zn(OH)C_2H_5 \rightarrow HOZnOZnOH + •C_2H_5 \quad (14)$$

The enthalpies for the reaction of $•OZnC_2H_5$, •OZnOH, and •OH with $Zn(C_2H_5)_2$ are −38.4, −38.2, and −36.9 kcal/mol, respectively, at B3LYP/6-311+G(d,p). The enthalpies for corresponding reactions with $Zn(OH)C_2H_5$ are −31.5, −30.7, and −29.6 kcal/mol, respectively. The similarity in reaction enthalpies suggests that $•OZnC_2H_5$, •OZnOH, and related oxyzinc radicals should have reactivities comparable to hydroxyl radical. The structures and selected geometric parameters of the products **16**−**18** are shown in Figure 3. Subsequent reactions could build longer zinc oxide chains.

Formation of Linear and Cyclic Oligomers. The presence of oxyzinc radicals provides a mechanism for the growth of linear zinc oxide chains in the gas phase. Likewise, the addition of oxyzinc radicals to the surface can lead to the growth of the zinc oxide film. In an earlier study,[14] we showed that $Zn(OH)C_2H_5$ and $Zn(OH)_2$ readily form cyclic dimers and tetramers. Formation of cyclic structures with the surface can also lead to the growth of the zinc oxide film. The cyclic dimers of $Zn(OH)C_2H_5$ and $Zn(OH)_2$, **19** and **20** in Figure 3, are formed without barriers at the B3LYP/6-311G(d) level.[14] The present calculations show that the dimers are more stable than separated monomers by 32.1 and 35.7 kcal/mol at the B3LYP/6-311+G(d,p) level and 35.7 and 42.7 kcal/mol at the G2(MP2) level of theory. Elimination of C_2H_6 from the cyclic dimer **19** is endothermic by 16.0 kcal/mol at the B3LYP/6-311+G(d,p) level and leads to an open chain structure $HOZnOZnC_2H_5$, **17**. The corresponding elimination of H_2O from **20** leads to HOZnOZnOH, **18**, and is endothermic by 33.8 kcal/mol. These ring opening reactions probably occur with significant barriers. Whether cyclic or linear oligomers will be formed in the gas phase will depend on the relative concentrations of $Zn(C_2H_5)_2$, $Zn(OH)(C_2H_5)$, $Zn(OH)_2$, and the associated oxyzinc radicals.

Free Energy Profiles. The relative free energy for the various intermediates in the gas-phase radical mechanism were calculated at the B3LYP/6-311+G(d,p) and G2(MP2) levels of theory at 700 K and pressures of 10 Torr and 1 atm. The low pressure is typical of many CVD processes, but there is interest in moving toward atmospheric pressure processes. The calculated free energy data are collected in Table 2 and summarized in Figure 5. Under these conditions, most of the complexes are not bound in terms of free energy. The formation of hydroxyl radical from ethyl radical and water has a large free energy barrier and may be the rate-determining step in this mechanism. Although the reaction of $•OH + Zn(C_2H_5)_2$ has no enthalpy barrier, it will have one on the free energy surface. If the variational transition state is early along the reaction path and the potential energy changes very little, the free energy of the variational transition state should be similar to or lower than that for the $H_2O +$

•C_2H_5 → C_2H_6 + •OH transition state, which has a very small reverse barrier. The calculated free energy for the reaction of $Zn(C_2H_5)_2 + H_2O \rightarrow Zn(OH)C_2H_5 + C_2H_6$ is −23 kcal/mol. The formation and reaction of the second hydroxyl radical proceed by lower free energy barriers than the first set of reactions. The overall reaction of $Zn(C_2H_5)_2 + 2H_2O \rightarrow Zn(OH)_2 + 2C_2H_6$ has a calculated free energy change of −38 kcal/mol. The calculated free energies indicate that formation of linear and cyclic dimers of $Zn(OH)C_2H_5$ and $Zn(OH)_2$ is favorable under CVD conditions.

The calculated free energy barrier (40.6 and 44.5 kcal/mol at B3LYP/6-311+G(d,p) and G2(MP2)) for $Zn(C_2H_5)_2 + H_2O \rightarrow Zn(OH)C_2H_5 + C_2H_6$ via the radical mechanism discussed in the present paper is comparable to the free energy barrier for the closed shell mechanism for the direct addition of water to diethyl zinc investigated in our previous paper (46.5 and 41.7 kcal/mol at B3LYP/6-311+G(d,p) and G2(MP2)). For the second step, $Zn(OH)C_2H_5 + H_2O \rightarrow Zn(OH)_2 + C_2H_6$, the calculated free energy barriers for the radical mechanism (17.1 and 21.8 kcal/mol at B3LYP/6-311+G(d,p) and G2(MP2)) are lower than for the first step and are lower than the corresponding free energy barrier in the closed shell mechanism (33.9 and 28.8 kcal./mol at B3LYP/6-311+G(d,p) and G2(MP2)). Since the barriers for the rate-limiting first hydrolysis are comparable, temperature should affect these reaction rates similarly. However, higher temperatures would increase the rate of the initiation reactions, thereby favoring the radical mechanism. Both the direct addition of water to diethyl zinc and the corresponding propagation steps for the radical mechanism are bimolecular; hence the effect of pressure on these reactions should be similar. However, higher pressures would enhance the termination steps and thus disfavor the radical mechanism.

Conclusions

In this study, we have examined some of the gas-phase reactions involved in the radical mechanism for zinc oxide CVD. Ethyl radical and hydroxyl radical are taken as the chain carriers. The direct or indirect reaction for the formation of OH radical from ethyl radical and water is probably the rate-limiting step. Addition of •OH to $Zn(C_2H_5)_2$ has no enthalpy barrier. For the rate-limiting first hydrolysis step, the free energy barrier for the radical mechanism is similar in magnitude to that obtained for the closed-shell mechanism studied earlier. High temperatures and low pressures will favor the radical mechanism because of their effect on the initiation and termination reactions.

Acknowledgment. This work was supported by a grant from the National Science Foundation (Grant CHE 0512144). The authors thank C&IT and ISC at Wayne State University for computer time. We wish to thank Stanley M. Smith for helpful discussions in the early phase of this study.

Supporting Information Available: Tables showing geometries optimized by B3LYP/6-31G(d). This material is available free of charge via the Internet at http://pubs.acs.org.

CM052314X